Flux distribution in superconducting films with holes

J. I. Vestgården, D. V. Shantsev, Y. M. Galperin, and T. H. Johansen
Department of Physics and Center for Advanced Materials and Nanotechnology, University of Oslo, P.O. Box 1048 Blindern, 0316 Oslo, Norway
(Received 28 August 2007; published 25 January 2008)

Flux penetration into type-II superconducting films is simulated for transverse applied magnetic field and flux creep dynamics. The films contain macroscopic nonconducting holes, and we introduce the holes in the simulation formalism by reconstruction of the magnetic field change inside the holes. We find that the holes induce a region of reduced flux density extending toward the nearest sample edge, in addition to the parabolic *d* lines. The region of reduced flux density is due to compression of current streamlines and is accompanied by a significantly enhanced flux traffic. The results are compared to and found to be in good agreement with experimental magneto-optical images of $YBa_2Cu_3O_x$ films including holes and slits.

DOI: 10.1103/PhysRevB.77.014521 PACS number(s): 74.25.Ha, 74.78.Bz, 74.25.Op

I. INTRODUCTION

The behavior of vortex matter in superconductors can, to a large degree, be controlled by introducing artificial defects. It has been known for a long time that randomly distributed defects, created, e.g., by neutron irradiation, allow a dramatic enhancement of the critical current density j_c. One may reach more specific goals by tuning the arrangement of artificial defects. In particular, experiments on superconducting thin films have revealed a large number of interesting effects, including matching effects,[1] noise reduction in superconducting quantum interference devices,[2] rectified vortex motion,[3,4] anisotropy of j_c,[5] and vortex guidance.[6]

In parallel with the experimental progress, the theoretical understanding of how artificially created patterns interact with vortex matter is also developing. Interaction between a single vortex and a cylindrical cavity was considered for bulk superconductors within the London approximation in Ref. 7. This work extends the classical paper (Ref. 8) predicting the maximal number of flux quanta that can be trapped by a single hole. Current distribution around a one-dimensional array of holes was calculated within the Ginsburg-Landau theory in Ref. 6. A realistic model should also take into account the strong pinning of vortices in the superconducting areas around the artificial defects. When the defect size is much larger than the London penetration depth, one can consider the average vortex density B rather than individual vortices. Such an approach was used in Refs. 9–11 to determine the current and flux distributions around corners, defects, and grain boundaries for creep dynamics. However, these theoretical works consider a *bulk* superconductor, while most experiments are on patterned *thin films*.[1–6] The dynamics of films is more complicated due to nonlocal electrodynamics.[12] This means that analytical results are difficult to obtain and one must instead rely on computer simulations, such as the flux penetration into a thin film with a two-dimensional array of holes simulated in Ref. 13. It allowed to explain an asymmetrical flux penetration by asymmetry in the hole shapes. At the same time, the case of an individual hole in a thin film has not yet been carefully analyzed. A main purpose of the present work is to acquire details of flux and current distributions in a superconducting strip with one individual hole.

An approximate picture of the current distribution around a nonconducting hole can be obtained within Bean's critical state model.[14] In the Bean model, current streamlines are added from the edge with equal spacing, representing the critical current density. The presence of a hole forces the current to flow around it and hence pushes the flux front deeper into the sample. Both holes and sample corners give rise to the so-called *d* lines where the current changes direction discontinuously.[15] They are seen as dark lines[16] in images that show magnetic flux distributions.[17,18] For example, 90°corners give 45° straight *d* lines[19] while semicircular indentations of the edge give parabolic *d* lines.[20] The magneto-optical image of Fig. 1 shows *d* lines spreading out from a circular hole toward the flux-free region. The same hole also introduces another pattern: a darkened region starting from the hole and extending *toward the edge*. This pattern is similar to the one observed by Eisenmenger *et al.*[21] The pattern does not fit with the common interpretation of the Bean

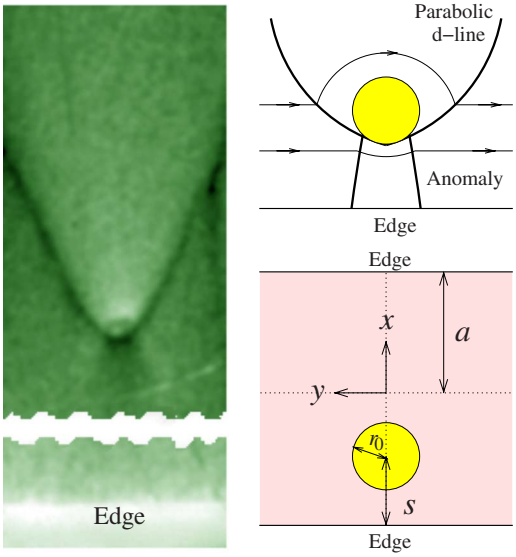

FIG. 1. (Color online) Left: Magneto-optical image showing details of B_z near a hole. Note the parabolic *d* lines going upward and a dark area going downward from the hole. Right: a sketch of the strip with a circular hole indicating how peculiarities in the flux distribution are related to bending of the current streamlines. Notations: film half-width is a, distance from the edge to the hole center is s, and the hole radius is r_0.

model, which leaves the the currents between the hole and the edge unperturbed. Reference 21 discusses how to reinterpret the Bean model and explain the observed pattern as a second parabolic d line. In this work, we will go further and do full dynamical simulation of flux penetration taking into account the nonlocal electrodynamics of films as well as flux creep. The simulated flux distributions are compared with magneto-optical images of patterned thin films, and both the experiment and the simulation reproduce the pattern of Ref. 21. Our results suggest that the observed anomaly is due to compression of current streamlines, rather than Bean-model d lines.

II. MODEL

A. Single-connected superconductors

Consider a type-II superconducting thin film placed in an increasing transverse magnetic field. The superconductor responds by generating screening currents to shield its interior. The current density is the highest at the edges where the Lorentz force eventually overcomes the pinning force, leading to penetration of flux. According to the Bean model, the vortices move only when the local current density exceeds the critical value j_c. A more realistic model for flux penetration also allows for flux creep at $j<j_c$. Macroscopically, flux creep is introduced through a highly nonlinear current voltage relation,[19,22]

$$\mathbf{E} = \rho_0 \left(\frac{j}{j_c}\right)^{n-1} \mathbf{j}, \tag{1}$$

where $\mathbf{E}$ is electric field, ρ_0 a resistivity constant, $\mathbf{j}$ is current density, and n is the creep exponent. For thin films of $YBa_2Cu_3O_x$, n is typically in the range from 10 to 70 depending on temperature and pinning strength.[23]

Flux dynamics of single-connected type-II superconductors in transverse geometry has been described thoroughly by Brandt. This work uses the same formalism and hence we only give a short summary of the simulation basics, mainly following Refs. 19, 24, and 25. The next section will be devoted to modifications of the formalism for multiply-connected samples.

For films, it is a great simplification to work with the sheet current $\mathbf{J}(\mathbf{r})=\int_{-d/2}^{d/2} dz \mathbf{j}(\mathbf{r},z)$, $\mathbf{r}=(x,y)$, instead of the current density $\mathbf{j}$. This is justified as long as thickness d is small compared to the in-plane dimensions but much larger than the London penetration depth λ. Finite λ can be handled with a small modification of the algorithm.[25] Since the current is conserved, $\nabla\cdot\mathbf{J}=0$, it can be expressed as $\mathbf{J}=\nabla\times\hat{z}g$, where $g=g(\mathbf{r})$ is the local magnetization.[24]

For single-connected thin films, the Biot-Savart law can be formulated as

$$B_z(\mathbf{r},z)/\mu_0 = H_a + \int_A d^2r' Q(\mathbf{r},\mathbf{r}',z) g(\mathbf{r}'), \tag{2}$$

where H_a is the applied magnetic field and A is the sample area. The kernel Q represents the field generated by a dipole of unit strength,[19]

$$Q(\mathbf{r},\mathbf{r}',z) = \frac{1}{4\pi}\frac{2z^2-(\mathbf{r}-\mathbf{r}')^2}{[z^2+(\mathbf{r}-\mathbf{r}')^2]^{5/2}}. \tag{3}$$

We discretize the kernel on an equidistant grid with grid points r_i and weights w and obtain[25]

$$Q_{ij} = \delta_{ij}\left(C_i/w + \sum_l q_{il}\right) - q_{ij}, \tag{4}$$

where $q_{ij}=1/4\pi|\mathbf{r}_i-\mathbf{r}_j|^3$ for $i\neq j$ and $q_{ii}=0$. The function C depends on the sample geometry. It is given as

$$C(\mathbf{r}) = \int_{\text{outside}} \frac{dr'^2}{4\pi|\mathbf{r}-\mathbf{r}'|^3}. \tag{5}$$

The time evolution of g comes from the inverse of Eq. (2),

$$\dot{g}(\mathbf{r}) = \int_A d^2r' Q^{-1}(\mathbf{r},\mathbf{r}')[\dot{B}_z(\mathbf{r}') - \mu_0\dot{H}_a], \tag{6}$$

where Q^{-1} for the discrete problem is the matrix inverse of Eq. (4). Here, $\dot{B}_z$ is by Faraday's law given as

$$\dot{B}_z(\mathbf{r}) = -(\nabla\times\mathbf{E})_z = \nabla\cdot\left(\frac{\rho}{d\mu_0}\nabla g\right), \tag{7}$$

with $\rho=\rho_0|\nabla g/J_c|^{n-1}$ obtained from Eq. (1). The right-hand side of Eq. (6) is expressed only by g and H_a so that time evolution of g can be found by integrating the equation numerically.

B. Superconductors with holes

For macroscopic, arbitrarily shaped, single-connected, type-II superconducting films, flux dynamics is fully described by Eq. (6). This basic equation can also be used for multiply-connected samples, but in that case, one needs to specify the dynamically changing value of g at the hole boundary. In Refs. 13 and 26, this value was set to the lowest value of g along the hole perimeter. This method turned out to be quite feasible but unfortunately, it cannot reproduce the discussed pattern of Fig. 1. Moreover, it also introduces unphysical net flux into the hole before the flux front has reached it.

A completely different approach is to consider the holes as part of the sample but ascribe to them the large Ohmic resistance or strongly reduced J_c.[27] Then, Eq. (6) applies to the whole sample including the holes, while the material law [Eqs. (1) and (7)] is spatially nonuniform. This approach is physically justified, but numerically challenging due to huge electric fields and field gradients, since the time step required for stability goes as $\Delta t\sim 1/E_{\max}$, where $E_{\max}$ is the maximum electric field inside the superconductor.[19] In addition, there will still remain small but nonzero currents flowing within the holes.

In this work, we propose an approach that does not require any additional assumptions, though requires a larger computational time. In this approach, the integration in Eq. (6) is extended over the whole sample area including the holes. Then, the dynamics of g is described by the equation

$$\dot{g}(\mathbf{r}) = \int_A d^2r' Q^{-1}(\mathbf{r},\mathbf{r}')[\dot{B}_z^{(s)}(\mathbf{r}') + \dot{B}_z^{(h)}(\mathbf{r}') - \mu_0 \dot{H}_a], \quad (8)$$

where A is the sample area including the hole. Here, we present $\dot{B}_z$ as a sum $\dot{B}_z^{(h)} + \dot{B}_z^{(s)}$, where $\dot{B}_z^{(h)}$ is nonzero only in the hole and $\dot{B}_z^{(s)}$ is nonzero only within the superconducting areas. Moreover, $\dot{B}_z^{(s)}$ is calculated in the straightforward way using Eq. (7). The other term, $\dot{B}_z^{(h)}$, is defined by two conditions. First, current must not flow beyond the superconducting areas, i.e., $\dot{g}$ is spatially constant within the hole. Second, the total solution satisfies Faraday's law,

$$\int_{\text{hole}} d^2r \dot{B}_z = -\int_{\text{hole edge}} d\mathbf{l} \cdot \mathbf{E}. \quad (9)$$

Thus, the role of Faraday's law is that it determines the value of $\dot{g}^{(h)}$ inside the hole, which, in general, is nonzero and time dependent.

In order to find the $\dot{B}_z^{(h)}$ that satisfies the two conditions, we use an iteration scheme. An initial guess, $\dot{B}_z^{(h,0)}$, is substituted into Eq. (8) to find $\dot{g}^{(h,0)}$, which is spatially nonconstant. The next approximation is found as

$$\dot{B}_z^{(h,1)}(\mathbf{r}) = \dot{B}_z^{(h,0)}(\mathbf{r}) - \int_{\text{hole}} d^2r' Q(\mathbf{r},\mathbf{r}')\dot{g}^{(h,0)}(\mathbf{r}') + K^{(0)}, \quad (10)$$

where the constant $K^{(0)}$ is chosen so that Eq. (9) is satisfied. Here, $\dot{B}_z^{(h,1)}$ is then inserted into Eq. (8) to find $\dot{g}^{(h,1)}$. This $\dot{g}^{(h,1)}$ is, in general, also spatially nonconstant, but when the procedure is repeated, $\dot{g}^{(h,n)}$ becomes more uniform with every new iteration. A smart choice of $\dot{B}_z^{(h,0)}$ is the final value at the previous time step, $\dot{B}_z^{(h,0)}(\mathbf{r},t) = \dot{B}_z^{(h,n)}(\mathbf{r},t-\Delta t)$. With this choice, only a couple of iterations are sufficient.

Note that the scheme presented here is in no way bound to the particular formulation of the kernel [Eq. (4)]. It can be used for any formulation as long as both the forward and inverse relations between $\dot{g}$ and $\dot{B}_z$ are known. Further mathematical details are in Appendix.

III. STRIP WITH A CIRCULAR HOLE

In this section, Eq. (8) is solved for an infinite superconducting strip in linearly increasing magnetic field. The strip is modeled using periodic boundary conditions in the y direction, and examples of magnetic field distributions are given in Fig. 2. In the upper part, one observes regular flux penetration with maximum of B_z at the edges. Flux penetration in the lower half is strongly affected by the presence a small, circular, nonconducting hole, where the flux distribution is perturbed in a region that significantly exceeds the hole dimensions.

The left image of Fig. 2 is at low field, when the flux front has not reached the hole yet. In this case, the hole shows up as a field dipole, in agreement with magneto-optical observations, cf. Refs. 21 and 29. Namely, there is positive field at the farther side of the hole and a negative field at the side

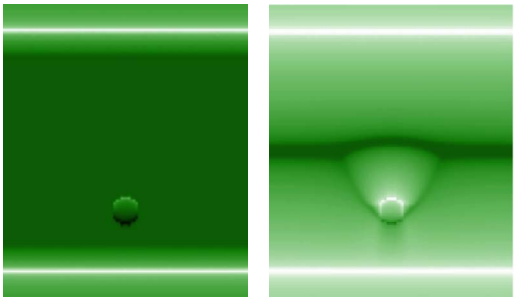

FIG. 2. (Color online) Simulated magnetic field distribution in a long strip, plotted in the style of magneto-optical images, where the intensity represents B_z. At small applied field (left), the hole produces a field dipole and at large field (right); one can see the parabolic d lines and a dark region between the hole and the edge, cf. the experimental image (Fig. 1); $r_0/a=0.1$, $s/a=0.5$, $n=19$, $H_a/J_c=0.2$ (left) and 1 (right), and $\mu_0\dot{H}_a=\rho_0 J_c/ad$.

closer to the film edge. The negative fields shrink when the flux front reaches the hole, but the asymmetry of the flux distribution inside the hole remains, as seen in the right image. As expected, the front becomes distorted so that the penetration is significantly deeper in the vicinity of the hole. For the full penetration image of Fig. 2, one also clearly sees the d lines as dark lines originating at the hole and directed toward the middle of the strip. Such d lines were described in Ref. 15 within the Bean-model framework, and they are called d lines because current changes direction discontinuously there. The discontinuity is most clearly seen in current streamline plot of Fig. 3 (left). For the Bean model, d lines from circular holes are parabolic and by convention d lines from small holes inside superconductors are often called parabolas. In the presence of flux creep, the change of current direction is smeared, as follows from Fig. 3 (right). However, the d lines are still clearly visible, at least for $n \gg 1$.

Comparing the two panels of Fig. 3, we notice a qualitative difference between the current flow in the bulk Bean model and for films under the creep. In the Bean model, the current density is everywhere constant, and all the current that is blocked by the hole turns toward the strip center. The

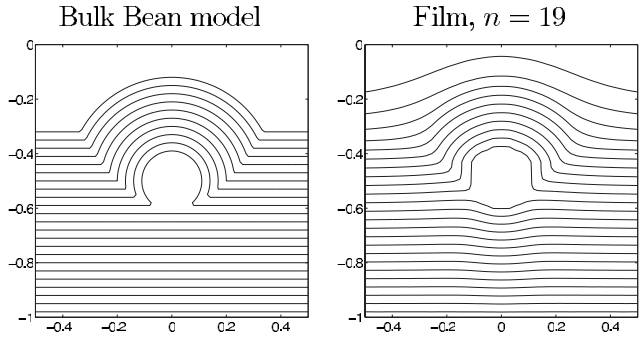

FIG. 3. Details of current streamlines near a circular hole for a slab in the Bean model (left) and for strip simulated with finite n (right). Only lower half of the slab and/or strip is shown. There are two features worth noticing for the strip result. First, the additional shielding currents in the flux-free region, and second, the bending and compression of streamlines between hole and edge.

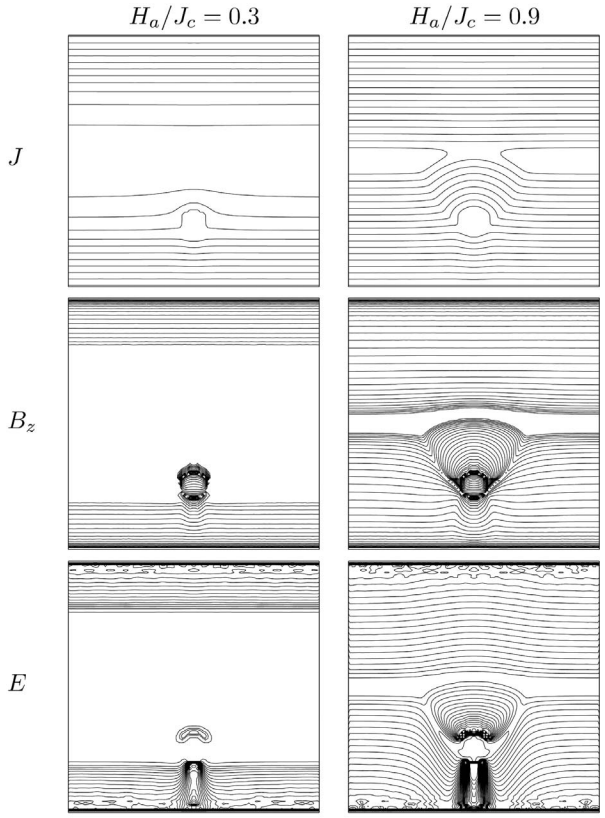

FIG. 4. Simulation results for a strip with a hole: the current streamlines (top), B_z contour lines (middle), and E contour lines (bottom). Note that the electric field is greatly enhanced in the channel between the hole and the edge (Ref. 28); H_a/J_c=0.3 and 0.9. The remaining parameters are the same as for Fig. 2.

region between the hole and the edge is hence unaffected by the presence of the hole. For films and creep dynamics, this is no longer true and a certain fraction of the current will force its way here. As a result, the current density is enhanced which is seen as denser streamlines in Fig. 3 (right). Since the streamlines bend, they create the feature visible in the flux distribution of Fig. 2: a slightly darkened region starting at the hole and widening toward the edge. This feature can also be observed experimentally, cf. Fig. 1. It was analyzed in detail in Ref. 21 and interpreted in terms of the Bean model as additional parabolic d lines. Our experiment and simulations suggest a different interpretation. We believe that one should speak about an *area* of reduced flux density rather than new d lines. Moreover, the appearance of this area is due to *locally enhanced* current density, hence it cannot be explained within the Bean model, postulating $J=J_c$. An enhanced current density also implies a strongly enhanced electric field. This is clearly seen in Fig. 4 showing the contour lines of E. A locally enhanced E means that there is an exceptionally intensive traffic of magnetic flux through the channel between the edge and the hole. The channel width is approximately given by the hole diameter but increases slightly toward the edge. The width depends, in general, on the distance to the edge and the creep exponent n. Both larger distance and smaller n tend to make the channel wider.

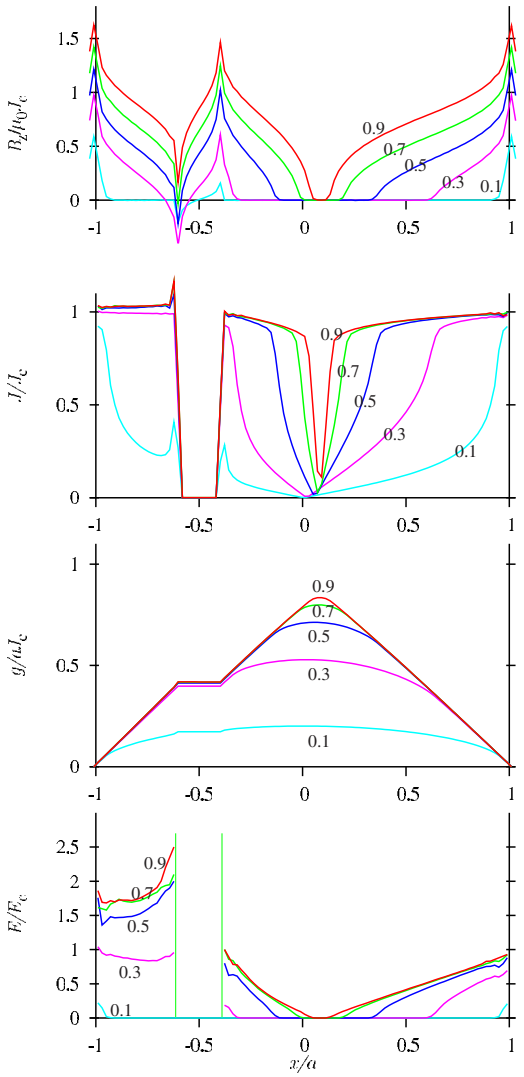

FIG. 5. (Color online) Profiles of B_z, J, g, and E through y=0 for a strip with a hole. The curves correspond to applied fields H_a/J_c=0.1, 0.3, 0.5, 0.7, and 0.9, as indicted in the figures, and with $E_c=\rho_0 J_c/d$. The remaining parameters are the same as for Fig. 2.

After arrival to the hole, the flux is further directed in the fan-shaped region between the d lines. Electric field within this region is also relatively high, again implying an intensive flux traffic. This situation is similar to the case of a semicircular indentation at the sample edge considered in Refs. 20, 30, and 31 The hole thus strongly rearranges trajectories of flux flow.

The above discussion is further confirmed by profiles of B_z, J, g, and E through the line y=0 shown in Fig. 5. The J profiles show features commonly observed in strips,[32] i.e., plateaus with values $\sim J_c$ in the penetrated regions and shielding currents with $J<J_c$ in the Meissner regions. The profiles show clearly the enhanced J and E between the edge and the hole. It is also interesting to see the negative B_z for low values and how the negative values gradually vanish when the main flux front gets in contact.

Figure 6 shows the total flux in a circular hole, $\Phi_h = \int_{\text{hole}} d^2 r B_z$, as a function of the applied field H_a for various

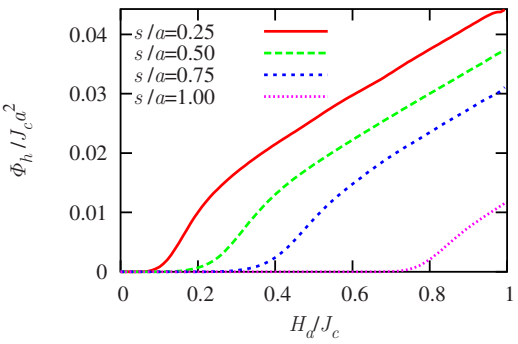

FIG. 6. (Color online) Total flux inside the hole, $\Phi_h = \int_{\text{hole}} d^2r\, B_z$, as a function of H_a for various distances s from the edge. For low fields, Φ_h is zero since the flux front has not reached the hole yet. For high fields, Φ_h grows linearly with H_a since the strip is saturated with $J \approx J_c$. Hole radii are $r_0/a = 0.1$. The remaining parameters are the same as for Fig. 2.

distances between the hole and the edge. In the beginning, $\Phi_h \approx 0$, until the main flux front is in contact with the hole. Then, it starts to increase. For high fields, Φ_h grows almost linearly with H_a at a universal growth rate determined by the hole area. The linear rate is not just the case for small holes in strips but has also been found for, e.g., ring geometry.[33] Note that for small fields, Φ_h is close to but not exactly zero. The reason is the creation of two additional flux fronts: one positive toward the flux-free region and one negative toward the edge, as also seen in Fig. 5. Only when integrating B_z over a larger area that includes this additional penetration, one finds that the total flux is exactly zero.[34] This integral is also a good consistency check of the boundary condition implementation, since an incorrect value of $g^{(h)}$ tends to introduce a net, unphysical flux in the hole.

IV. COMPARISON WITH EXPERIMENT

A. Circular hole

The magneto-optical image of Fig. 1 is the typical result of having a natural defect of circular shape located inside a sample. The image has been cut due to the relatively large distance between this hole and the edge, and it shows only the details near the hole. The strip-shaped sample is subject to an increasing external field and shows a clearly visible main parabolic d line. In particular, there are two details worth noticing in the magneto-optical image compared to the simulation image of Fig. 2, corresponding to nearly full penetration. First, both images show the same darkened region extending toward the edge. Second, the magnetic field distributes in the same asymmetric way near the hole, where one finds the highest field value along the part of the hole perimeter that is most distant from the edge.

B. Square with two slits

Figure 7 shows a square with two slits. The figure contains a magneto-optical image of a $YBa_2Cu_3O_x$ film and a corresponding simulated flux distribution. The experimental film thickness is 250 nm and side lengths are 2.5 mm. The

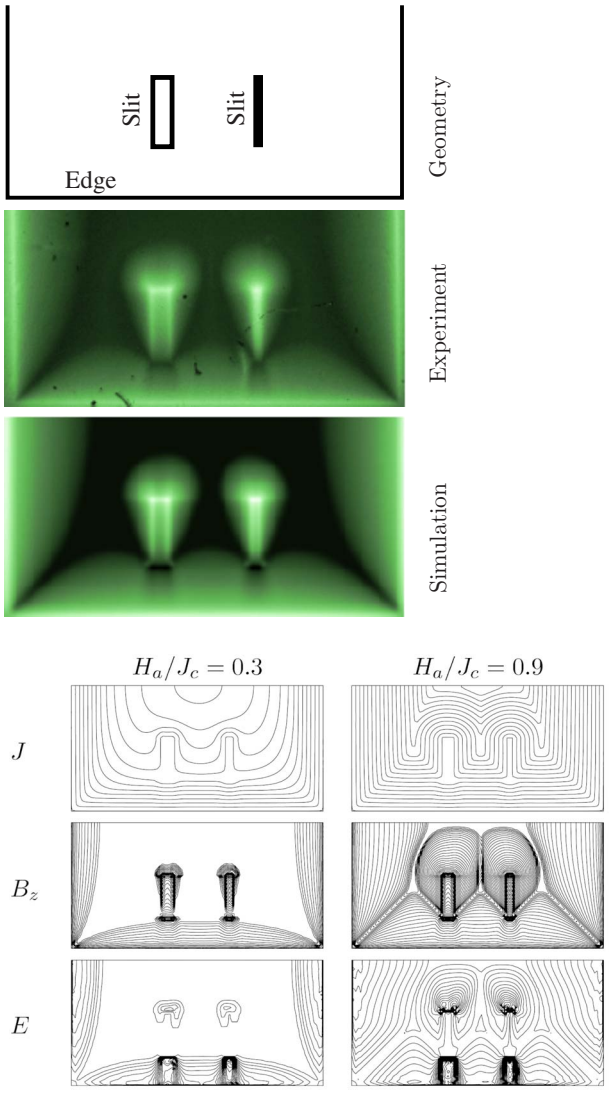

FIG. 7. (Color online) A square with two slits (only the lower half is shown). Top: sample sketch, experimental magneto-optical image of $YBa_2Cu_3O_x$ film, and simulated magnetic field distribution. Bottom: current streamlines, B_z and E contour lines at $H_a/J_c = 0.3$ and 0.9, with $n = 19$ and $\mu_0 \dot{H}_a = \rho_0 J_c / ad$.

two slits have been cut out with a laser. Details of the film preparation can be found elsewhere.[35]

The experiment and simulation show a great similarity both in large and in the details. The flux density is considerably enhanced everywhere along the slit edges and reaches the maximal values at the upper corners. Our main result found for circular holes holds true also for rectangular slits. Namely, we again find a distinct dark region starting at the slit and widening toward the edge. A difference compared to circular holes is the appearance of slightly brightened lines or regions near the upper corners of the slits. These appear due to concave current turns and they can also arise in superconductors of other shapes having concave corners, e.g., in crosses.[30]

There also exist a few minor discrepancies between flux distributions obtained in the simulations and in the experiment of Fig. 7. The most notable is the details of the region of reduced B_z at the side of slits close to the edge. The values

of B_z appear to be less in the simulation than in experiment. This might be caused by simplifications, such as the disregarded B dependency of the material law or the simplification of using the sheet current instead of the true current density.

The bottom part of Fig. 7 shows details of the simulated J, B_z, and E. Note the enhanced J and E between the slit and the edge, exactly as for the circular hole. In addition, the figure shows a complicated flux distribution and a rich set of d lines at full penetration.

V. SUMMARY

We have proposed a method for treating boundary conditions of nonconducting holes inside macroscopic, type-II superconducting films. The key point is to reconstruct the, at first, unknown $\dot{B}_z$ inside the holes at each time step of the simulation. The method is capable of handling any number of holes of arbitrary shape.

The simulations of flux dynamics assuming a material law $E \sim j^n$ reproduce very well flux distributions observed by magneto-optical imaging in $YBa_2Cu_3O_x$ films for circular holes as well as rectangular slits. In particular, they demonstrate a region of reduced flux density in the superconductor originating from the hole and/or slit and extending toward the nearest sample edge. This region is not a conventional d line but rather a region of enhanced current density and more intensive traffic of flux.

ACKNOWLEDGMENTS

We thank C. Romero-Salazar and Ch. Jooss for fruitful discussions and M. Baziljevich for experimental data on Fig. 7. This work was supported financially by The Norwegian Research Council under Grant No. 158518/431 (NANOMAT) and by FUNMAT@UIO.

APPENDIX: NUMERICAL DETAILS

The simulations are run on a $N \times N$ square grid. The creep exponent and the ramp rate are $n=19$ and $\mu_0 \dot{H}_a = \rho_0 J_c / ad$, a regime in which creep is low but not negligible. Changing n would only do quantitative changes to the results. For small exponents, the plateaus of current profiles, like Fig. 5, would be less flat, and there would also be more current compressed between the holes and the edge.

The main limiting factor of the simulations is memory consumption since the kernel matrix Q [Eq. (4)] has dimension $N^2 \times N^2$. The simulations are run with $N=100$ grid points, which yields a kernel matrix of dimension 5000×5000, when the sample symmetry has been exploited.[19]

The kernel Q in Eq. (4) depends explicitly on the sample shape. Since the strip is infinite in the y direction, Q should be computed via an infinite sum over strip segments. However, a good approximation is achieved with only one segment on each side of the "main" strip. The strip segments further away contain zero net current and the dipolelike character means that they have a negligible effect. A good accuracy of this approximation was checked by comparing the Meissner state width b, obtained for very high n with the analytical film Bean-model result,[36] $b = a/\cosh(\pi H_a / J_c)$.

The reconstruction of $\dot{B}_z$ inside the hole [Eq. (10)] needs not to use the full Q from Eq. (4). A better choice is to use a smaller kernel $\tilde{Q}$ also generated with Eq. (4), but only including points inside the hole. Fast convergence of Eq. (10) is achieve by ignoring currents at the hole perimeter, which means that $\tilde{Q}$ should use $C(\mathbf{r})=0$.

The most difficult numerical problem in our method is the calculation of the electric field at the boundary in Eq. (9). The electric field is given by the power law [Eq. (1)], and is largely fluctuating between neighboring grid points. A stable way to handle this is to take the average of only the most significant values of E and use $2\pi r$ and πr^2 for the hole circumference and area.

[1] V. V. Moshchalkov, M. Baert, V. V. Metlushko, E. Rosseel, M. J. Van Bael, K. Temst, Y. Bruynseraede, and R. Jonckheere, Phys. Rev. B **57**, 3615 (1998).
[2] R. Wördenweber and P. Selders, Physica C **366**, 135 (2002).
[3] C. C. de Souza Silva, J. Van de Vondel, M. Morelle, and V. V. Moshchalkov, Nature (London) **440**, 651 (2006).
[4] J. Van de Vondel, C. C. de Souza Silva, B. Y. Zhu, M. Morelle, and V. V. Moshchalkov, Phys. Rev. Lett. **94**, 057003 (2005).
[5] M. Pannetier, R. J. Wijngaarden, I. Fløan, J. Rector, B. Dam, R. Griessen, P. Lahl, and R. Wördenweber, Phys. Rev. B **67**, 212501 (2003).
[6] R. Wördenweber, P. Dymashevski, and V. R. Misko, Phys. Rev. B **69**, 184504 (2004).
[7] H. Nordborg and V. M. Vinokur, Phys. Rev. B **62**, 12408 (2000).
[8] G. S. Mkrtchyan and V. V. Shmidt, Sov. Phys. JETP **34**, 195 (1972).
[9] A. Gurevich and J. McDonald, Phys. Rev. Lett. **81**, 2546 (1998).
[10] A. Gurevich and M. Friesen, Phys. Rev. B **62**, 4004 (2000).
[11] M. Friesen and A. Gurevich, Phys. Rev. B **63**, 064521 (2001).
[12] E. H. Brandt, Phys. Rev. B **46**, 8628 (1992).
[13] D. G. Gheorghe, M. Menghini, R. J. Wijngaarden, S. Raedts, A. V. Silhanek, and V. V. Moshchalkov, Physica C **437–438**, 69 (2006).
[14] C. P. Bean, Rev. Mod. Phys. **36**, 31 (1964).
[15] A. M. Campbell and J. Evetts, *Critical Currents in Superconductors* (Taylor & Francis, London, 1972).
[16] What is dark and bright in magneto-optical images depends on experimental setup. In this paper, dark means low field and bright high field, which is the most common situation.
[17] T. Schuster, M. V. Indenbom, M. R. Koblischka, H. Kuhn, and H. Kronmüller, Phys. Rev. B **49**, 3443 (1994).
[18] C. Jooss, J. Albrecht, H. Kuhn, S. Leonhardt, and H. Kronmüller, Rep. Prog. Phys. **65**, 651 (2002).
[19] E. H. Brandt, Phys. Rev. B **52**, 15442 (1995).

[20] R. G. Mints and E. H. Brandt, Phys. Rev. B **54**, 12421 (1996).
[21] J. Eisenmenger, P. Leiderer, M. Wallenhorst, and H. Dötsch, Phys. Rev. B **64**, 104503 (2001).
[22] E. Zeldov, N. M. Amer, G. Koren, A. Gupta, and M. W. McElfresh, Appl. Phys. Lett. **56**, 680 (1990).
[23] J. Z. Sun, C. B. Eom, B. Lairson, J. C. Bravman, and T. H. Geballe, Phys. Rev. B **43**, 3002 (1991).
[24] E. H. Brandt, Phys. Rev. Lett. **74**, 3025 (1995).
[25] E. H. Brandt, Phys. Rev. B **72**, 024529 (2005).
[26] K. A. Lörincz, M. S. Welling, J. H. Rector, and R. J. Wijngaarden, Physica C **411**, 1 (2004).
[27] A. Crisan, A. Pross, D. Cole, S. J. Bending, R. Wördenweber, P. Lahl, and E. H. Brandt, Phys. Rev. B **71**, 144504 (2005).
[28] E inside the hole cannot be found from the material law and is simply set to zero in the plots. The correct E inside the hole must be found from Faraday's law (Ref. 37).
[29] V. V. Yurchenko, R. Wördenweber, Y. M. Galperin, D. V. Shantsev, J. I. Vestgården, and T. H. Johansen, Physica C **437–438**, 357 (2006).
[30] T. Schuster, H. Kuhn, and E. H. Brandt, Phys. Rev. B **54**, 3514 (1996).
[31] J. I. Vestgården, D. V. Shantsev, Y. M. Galperin, and T. H. Johansen, Phys. Rev. B **76**, 174509 (2007).
[32] T. H. Johansen, M. Baziljevich, H. Bratsberg, Y. Galperin, P. E. Lindelof, Y. Shen, and P. Vase, Phys. Rev. B **54**, 16264 (1996).
[33] Åge Andreas Falnes Olsen, T. H. Johansen, D. Shantsev, E.-M. Choi, H.-S. Lee, H. J. Kim, and S.-I. Lee, Phys. Rev. B **76**, 024510 (2007).
[34] E. H. Brandt, Phys. Rev. B **55**, 14513 (1997).
[35] M. Baziljevich, T. H. Johansen, H. Bratsberg, Y. Shen, and P. Vase, Appl. Phys. Lett. **69**, 3590 (1996).
[36] E. H. Brandt and M. Indenbom, Phys. Rev. B **48**, 12893 (1993).
[37] C. Jooss and V. Born, Phys. Rev. B **73**, 094508 (2006).